atmosphere

MDPI

Article

Evaluation of the Conversion Efficiency of Catalytic Convertors for Stoichiometric and Lean-Burn Methanol Engines

Laihua Shi [1], Chongyao Wang [2,*], Jianjian Kang [3], Lan Li [3], Xiaoliu Xu [1], Di Wu [3], Bing Liu [3] and Xin Wang [2]

[1] China Merchants Testing Vehicle Technology (Hefei) Co., Ltd., No. 9, JiangJunling East Road, Industry and Finance Demonstration Zone, HuaGang Town, Feixi County, Hefei 231241, China
[2] School of Mechanical Engineering, Beijing Institute of Technology, Zhongguancun South Street No. 5, Beijing 100081, China
[3] China Merchants Testing Vehicle Technology Research Institute Co., Ltd., Chongqing 401329, China
* Correspondence: 7520260095@bit.edu.cn

Abstract

Heavy-duty methanol engines are regarded as a promising low-carbon solution for commercial vehicle decarbonization, yet the comprehensive coupled characteristics of fuel consumption, multi-dimensional exhaust emissions, and the corresponding aftertreatment adaptability between stoichiometric and lean-burn technical routes remain insufficiently quantified, restricting the optimized application of methanol powertrains for China-VI emission compliance. To address this research gap, this study systematically investigates two China-VI compliant heavy-duty methanol engines with stoichiometric and lean-burn combustion strategies under cold-start and hot-start Worldwide Harmonized Transient Cycle. And a comparative analysis is conducted to clarify the differences in the fuel consumption, raw exhaust emission (including regulated pollutants, particulate matters, greenhouse gases, and unregulated pollutants), and the catalytic performance of aftertreatment systems between two engines with stoichiometric and lean-burn strategy. Results demonstrate that the lean-burn strategy achieves a 6% reduction in methanol fuel consumption compared with stoichiometric combustion, delivering superior fuel economy. In terms of regulated gaseous pollutants, both combustion strategies satisfy China-VI emission limits for CO and NO, while lean-burn combustion effectively lowers raw CO and NO emissions and reduces the purification pressure of aftertreatment systems. Non-methane Hydrocarbon emission under cold-start condition is identified as the primary compliance challenge, requiring a minimum aftertreatment conversion efficiency of 95%. Although lean-burn increases raw exhaust NMHC emission under hot-start condition, the post-catalyst emission could still meet the regulation limits. For particulate pollutants, lean-burn strategy realizes substantial reductions in both PM and PN emissions, which can meet emission standards without the corresponding aftertreatment system. In contrast, the stoichiometric combustion faces a risk of PN emission exceeding the regulation limit under cold-start conditions even with aftertreatment system. Additionally, lean-burn strategy optimizes greenhouse gas emission performance by cutting CO and CH_4 emissions. Regarding unregulated pollutants, lean-burn strategy increases raw exhaust unburned methanol and formaldehyde emissions, particularly under cold-start condition, but significantly inhibits NH_3 emission. This study quantitatively clarifies the performance trade-offs and adaptation advantages of lean-burn and stoichiometric strategy for heavy-duty methanol engines, providing fundamental data support and technical guidance for the low-carbon and low-pollution optimization of heavy-duty methanol vehicles.

Check for updates

Academic Editor: Jaroslaw Krzywanski

Received: 15 June 2026
Revised: 25 July 2026
Accepted: 28 July 2026
Published: 31 July 2026

Copyright: © 2026 by the authors. Licensee MDPI, Basel, Switzerland. This article is an open access article distributed under the terms and conditions of the Creative Commons Attribution (CC BY) license.

Keywords: heavy-duty vehicle; methanol engine; lean-burn; exhaust emission

1. Introduction

To alleviate environmental pollution and mitigate climate change, China proposed a carbon peaking and carbon neutrality strategy in 2020 [1]. As of May 2024, 151 countries have announced their carbon neutrality targets [2]. Carbon neutrality commitments are continuously expanding in coverage and gradually moving into the implementation phase. As a renewable fuel, methanol can be used for vehicles to facilitate the energy transition and support the carbon peaking and carbon neutrality strategy [3,4]. Methanol features high combustion efficiency, abundant raw material resources, mature production pathways, and low manufacturing costs. It remains liquid under ambient temperature and pressure, facilitating storage and transportation [5–7]. Furthermore, methanol synthesis powered by renewable energy such as solar power represents a promising pathway to reduce carbon emissions in the future. Compared with gasoline and diesel, methanol features low carbon content, high oxygen content, and simple chemical composition. Its combustion in engines thereby yields lower CO, CO_2, and NO_x emissions without sulfide pollutants [6]. Numerous studies have verified that methanol can achieve persistent and remarkable reductions in NO_x and particulate matter (PM) emissions from both light-duty and heavy-duty vehicles [8–10]. Therefore, methanol is regarded as a vital alternative fuel with prominent advantages in economic performance [11], energy efficiency [12], environmental sustainability [13], and operational safety [14].

However, unregulated emissions (e.g., unburned methanol and formaldehyde) are generated in the engine exhaust during methanol combustion, bringing additional environmental risks [15]. Zhao et al. [16] investigated the carbonyl emissions from vehicles fueled with methanol–gasoline blends (M15 and M100) under the New European Driving Cycle (NEDC). Results showed that formaldehyde emissions increased by two and four times for M15 and M100, respectively, and total carbonyl emissions increased by 3% and 104% for M15 and M100 compared with gasoline, respectively. Zhao et al. [17] further measured pollutant emissions from methanol–gasoline blends with varied methanol fractions under NEDC test conditions. Results showed that carbonyl compounds (particularly formaldehyde) in tailpipe emissions increased significantly with rising methanol blending ratios. Yao et al. [18] further confirmed this finding and indicated that higher engine speeds raised the in-cylinder combustion temperature and accelerated the partial oxidation of methanol, leading to the finding that formaldehyde emissions gradually increased with engine speed, while methanol emissions gradually decreased. Wang et al. [19,20] investigated regulated pollutants, unregulated pollutants, and particulate matter emissions from vehicles fueled with gasoline, M15, M25, M40, and M100 under the NEDC. Results showed that formaldehyde accounted for approximately 50% of carbonyl emissions from methanol combustion. Moreover, combustion of neat methanol (M100) increased formaldehyde emissions by 19.8% relative to gasoline. Su et al. [21] evaluated regulated pollutants, unregulated pollutants, and particle number emissions from a high-mileage China IV methanol taxi under the NEDC. The study indicated that unburned methanol is a major challenge for future methanol applications. Moreover, emissions of formaldehyde and unburned methanol rose more rapidly with catalyst aging than regulated pollutant emissions. The above studies indicate that unregulated pollutant emissions have become a critical issue restricting the development of methanol engines.

Furthermore, although CO_2 emissions from methanol fuel are theoretically lower than those from diesel, this advantage can be affected by multiple factors (including the thermal

efficiency of engines, ambient temperature, and other operating parameters). By analyzing the transient CO_2 emissions of five heavy-duty vehicles (one equipped with a stoichiometric methanol engine and four with lean-burn diesel engines), it was found that only two diesel vehicles produced higher CO_2 emissions, while the remaining diesel vehicles yielded lower CO_2 emissions than the stoichiometric methanol vehicle [22–24]. This indicates that the CO_2 emission advantage of stoichiometric methanol engines is insignificant, especially with the continuous improvement in diesel engine thermal efficiency. Duan et al. [24,25] measured the CO_2 emissions of stoichiometric methanol vehicles under cold-start and hot-start World Harmonized Transient Cycle (WHTC) conditions. The results showed that CO_2 emissions under cold-start conditions were significantly higher than those under hot-start conditions, with an increase of 2–5%. This reveals that the CO_2 emission advantage of stoichiometric methanol vehicles declines as ambient temperature decreases and may even turn into a disadvantage under low-temperature conditions, compared with lean-burn diesel vehicles. Therefore, improving the thermal efficiency of heavy-duty methanol engines is essential for emission reduction.

Lean-burn combustion is an effective strategy to improve thermal efficiency and reduce emissions in spark ignition engines [26,27]. The fuel properties of methanol allow a wider lean-burn limit compared with gasoline, making the combination of methanol and lean-burn combustion a feasible technical route for methanol engines [28–31]. Therefore, lean-burn methanol engines represent a promising technical pathway for heavy-duty vehicles.

Some studies have focused on the emission characteristics of lean-burn methanol engines. Ning et al. [32] investigated the lean-burn characteristics of a modified diesel engine operating in methanol direct injection spark ignition (DISI) mode under full throttle conditions. Results showed that regulated pollutants and CO_2 emissions decreased with increasing excess air ratio (λ). Wu et al. [33] compared the emission characteristics of an SI engine fueled with methanol and gasoline under idling conditions. The results further confirmed that methanol significantly reduced regulated pollutant emissions under lean-burn conditions and indicated that the high oxygen content of methanol improved the homogeneity of the air–fuel mixture, thus reducing pollutants from incomplete combustion. Gong et al. [34] explored the effect of λ on emissions of a high-compression-ratio spark ignition H_2/methanol dual-injection engine through numerical simulation. Results showed that the emissions of CO, formaldehyde, and unburned methanol increased with λ, while the emissions of NO decreased. These results indicate that lean-burn methanol engines exhibit advantages in regulated emissions but face a risk of increased unregulated pollutants.

In addition, some studies have focused on the reduction of unregulated pollutant emissions from lean-burn methanol engines. Gong et al. [35] studied the effect of injection timing on the concentration field of the stratified-charge mixture, combustion behavior, and emission characteristics of methanol engines under ultra-lean-burn conditions by simulation. Results showed that CO, unburned methanol, and soot emissions were significantly reduced at the optimal injection and spark timing, suggesting that ideal stratified-charge combustion was the key to reducing emissions. Gong et al. [36] explored the effects of intake temperature on mixture formation, combustion, and unregulated pollutant emissions of a direct injection spark ignition (DISI) methanol engine through numerical simulations. Results showed that increasing the intake temperature accelerated methanol evaporation and optimized in-cylinder mixture distribution, which promoted combustion and reduced emissions of formaldehyde and unburned methanol. These results indicate that the regulated pollutant emissions of lean-burn methanol engines can be efficiently reduced by optimizing engine parameters.

Although existing studies have partially revealed the emission characteristics of stoichiometric and lean-burn methanol engines, most investigations only focus on a single

combustion strategy. Systematic quantitative comparisons between these two combustion modes of heavy-duty methanol engines under identical transient WHTC test conditions covering both cold- and hot-start phases remain scarce, leaving a research gap in which the comprehensive performance trade-offs and inherent emission drawbacks of the two modes have not been fully clarified. Stoichiometric combustion represents the current mainstream technical route for commercial heavy-duty methanol vehicles. Nevertheless, its limitations in thermal efficiency, carbon emission performance, and unregulated pollutant control hinder the further market penetration of methanol engines. In contrast, lean-burn combustion is widely recognized as a promising technical route to improve thermal efficiency and reduce carbon emissions for future heavy-duty vehicles. Under such circumstances, an in-depth comparative evaluation of stoichiometric and lean-burn combustion is essential to support combustion strategy selection and technical upgrading of next-generation methanol engines.

Accordingly, this study systematically and quantitatively compares the fuel economy and exhaust emission performance of heavy-duty stoichiometric and lean-burn methanol engines under WHTC conditions. A wide range of exhaust pollutants are analyzed, including regulated gaseous pollutants, PM/particle number (PN), greenhouse gases, and unregulated emissions such as formaldehyde, unburned methanol, and ammonia. It aims to identify the respective strengths and potential limitations of the two combustion strategies and provide a fundamental reference for performance optimization and technical route development of future low-carbon heavy-duty methanol vehicles.

2. Methodology

2.1. Experimental Setup

This study was conducted based on the engine bench test method specified in the China VI heavy-duty vehicle emission regulations, with the schematic diagram of the experimental setup shown in Figure 1.

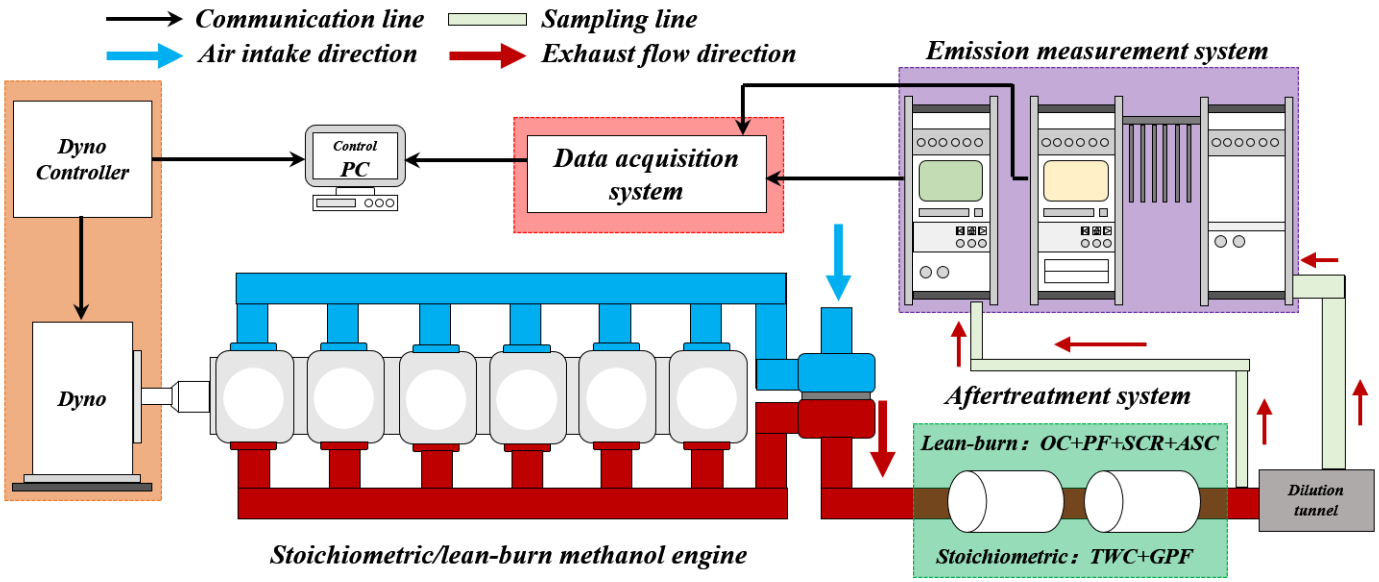


Figure 1. Schematic of the experimental system.

Two heavy-duty methanol engines developed to meet the China VI emission regulations were selected as the research objects. Both engines were designed for heavy-duty tractor-trailers and equipped with 6-cylinder, water-cooled and turbocharging systems, with the corresponding displacement, rated power and maximum torque of 13 L, 348 kW,

and 2185 N·m, respectively. The distinction between the two engines lies in their combustion strategies and aftertreatment configurations. One engine adopted a stoichiometric combustion strategy, coupled with three-way catalyst (TWC) and particulate filter (PF) aftertreatment systems, and achieved a compression ratio of 12.5:1. The other employed a lean-burn combustion strategy with an excess air ratio of 1.35. It was equipped with integrated aftertreatment systems, including an oxidation catalyst (OC), a particulate filter (PF), a selective catalytic reduction (SCR), and an ammonia slip catalyst (ASC) aftertreatment systems, and achieved a compression ratio of 14.5:1. The rated speed of the lean-burn engine was 1900 r/min, which was 100 r/min higher than that of the stoichiometric engine.

A HORIBA HD460 dynamometer (HORIBA, Ltd. Kyoto, Japan) was employed for engine bench testing, with speed and torque control accuracies of ±1 r/min and ±0.17%, respectively. Gaseous pollutants (excluding NH_3) were sampled using the bag sampling technique coupled with a full-flow constant-volume dilution system. A HORIBA MEXA-7200D emission analyzer (HORIBA, Ltd., Kyoto, Japan) was utilized to measure pollutant concentrations, with a full-scale measurement error of ±1.0%. NH_3 was directly sampled from the exhaust pipe and quantified via a HORIBA MEXA-ONE-FT-E analyzer (HORIBA, Ltd., Kyoto, Japan) equipped with Fourier transform infrared spectroscopy, with a measurement error of ±1.0%. Particulate matter (PM) and particle number (PN) emissions were sampled at the stable section of the constant-volume dilution tunnel but quantified through different analytical procedures. For PM measurement, the HORIBA DLS-7200E (HORIBA, Ltd., Kyoto, Japan) was adopted to conduct proportional constant-flow sampling. All PM samples were conditioned in a constant-temperature and constant-humidity weighing chamber for a minimum of 2 h before and after testing. Sample weighing was carried out using a Mettler Toledo XP2UV analytical balance, with a measurement error of 1 μg. PN concentrations were measured with the HORIBA MEXA-2000SPCS condensation particle counter (HORIBA, Ltd., Kyoto, Japan), which incorporated a two-stage dilution system containing an evaporation tube.

During the formal measurements, neat methanol (M100) and 92-octane gasoline were adopted as test fuels. It should be noted that gasoline was only supplied during the engine cold-start phase (when the coolant temperature was no more than 70 °C), aiming to improve the poor cold-start performance of methanol engines. Once the coolant temperature exceeded 70 °C, the fuel was automatically switched to methanol. An ACSW3000 intake air conditioning system maintained the engine intake conditions at a temperature of 25 ± 1 °C, a relative humidity of 30 ± 3%, and an absolute pressure of 100 ± 1 kPa. Subsequently, raw exhaust and post-catalyst emissions (covering regulated pollutants, particulate matter, greenhouse gases, and unregulated species) from the stoichiometric and lean-burn engines were measured under the WHTC, respectively. All measurements for both engines were repeated no fewer than two times to guarantee data repeatability.

2.2. Data Processing

In this study, all measured experimental data were systematically processed to quantitatively evaluate engine exhaust emissions and fuel consumption. Emission factors of all pollutants for each test were calculated using Equation (1). Fuel consumption and thermal efficiency were calculated using Equation (4) and Equation (5), respectively. The conversion efficiency of the aftertreatment system was calculated using Equation (6). It should be noted that when Equation (6) was adopted to determine the minimum conversion efficiency required to satisfy emission regulations, the catalyst-out pollutant concentration was set equal to the corresponding regulatory limit. For CO, the catalyst-out concentration was specified as 4000 mg/(kW·h). For NMHC, the catalyst-out concentration was specified as 160 mg/(kW·h). For NO_x, the catalyst-out concentration was specified as 460 mg/(kW·h).

Finally, the average values of the above-mentioned performance indexes, calculated from two groups of experimental results for the stoichiometric engine and three groups of experimental results for the lean-burn engine, were used for subsequent result analysis, while the corresponding standard deviation was also calculated using Equation (7) to guarantee the accuracy and validity of the obtained data.

$$EF_i = \frac{\sum \dot{m}_i}{W_{WHTC}} \tag{1}$$

In Equation (1), EF_i is the emission factor of pollutant i, with the unit of g/(kW·h). $\dot{m}_i$ is the mass flow rate of pollutant i, with the unit of g/s, which can be calculated using Formula (2) for gaseous pollutants and Formula (3) for particulate number, respectively. W_{WHTC} is the accumulated work during the whole *WHTC*, with the unit of kW·h.

$$\dot{m}_i = c_i \times \frac{M_i}{22.4} \times q_e \times \frac{1}{f} \times \frac{10^{-6}}{60} \tag{2}$$

In Equation (2), $\dot{m}_i$ is the mass flow rate of pollutant i, with the unit of g/s. c_i is the instantaneous concentration of pollutant i, with the unit of 10^{-6}. M_i is the molar mass of pollutant i, with the unit of g/mol. q_e is the volume flow rate, with the unit of L/min. f is the frequency of sampling, with the unit of Hz.

$$\dot{m}_{PN} = c_{PN} \times q_e \times \frac{1}{f} \times \frac{10^3}{60} \tag{3}$$

In Equation (3), $\dot{m}_{PN}$ is the number flow rate of particulate, with the unit of */s. c_{PN} is the concentration of particulate, with the unit of $*/cm^3$. q_e is the volume flow rate, with the unit of L/min. f is the frequency of sampling, with the unit of Hz.

$$BSFC = \frac{EF_{CO_2} \times \frac{12}{44} + EF_{CO} \times \frac{12}{28} + EF_{NMHC} \times \frac{12}{32} + EF_{CH_4} \times \frac{12}{16}}{\frac{12}{32}} \tag{4}$$

In Equation (4), *BSFC* is brake specific fuel consumption, with the unit of g/(kW·h). EF_{CO_2} is the emission factor of CO_2, with the unit of g/(kW·h). EF_{CO} is the emission factor of CO, with the unit of g/(kW·h). EF_{NMHC} is the emission factor of NMHC, with the unit of g/(kW·h). EF_{CH_4} is the emission factor of CH_4, with the unit of g/(kW·h).

$$\eta_{eng} = \frac{3600}{BSFC \times H} \times 100 \tag{5}$$

In Equation (5), η_{eng} is the thermal efficiency of engine, with the unit of %. *BSFC* is brake specific fuel consumption, with the unit of g/(kW·h). H is the calorific value of methanol, with the unit of kJ/g.

$$\eta_{aft} = \frac{EF_{in} - EF_{out}}{EF_{in}} \times 100 \tag{6}$$

In Equation (6), η_{aft} is the conversion efficiency of the aftertreatment system, with the unit of %. EF_{in} is the emission factor at the catalyst inlet, with the unit of g/(kW·h). EF_{out} is the emission factor at the catalyst outlet, with the unit of g/(kW·h).

$$\sigma = \sqrt{\frac{\sum_{i=1}^{n} (x_i - \overline{x})^2}{n}} \tag{7}$$

In Equation (7), σ is the standard deviation of the samples. x_i is the value of each sample. $\overline{x}$ is the average of total samples, and n is the number of the samples.

3. Results and Discussion

This section systematically investigates the energy utilization and exhaust emission characteristics of stoichiometric and lean-burn methanol engines under cold-start and hot-start conditions. First, fuel consumption and thermal efficiency are compared between these two engine configurations. Subsequently, raw exhaust emissions and post-catalyst emissions (including gaseous pollutants, particulate matter, greenhouse gases, and unregulated pollutants) from these methanol engines are assessed, alongside the catalytic performance of their respective aftertreatment systems.

3.1. Fuel Consumption

The methanol fuel consumption of stoichiometric and lean-burn engines was quantified using the carbon balance method, with the corresponding results summarized in Table 1. As illustrated in Table 1, the lean-burn engine exhibits pronounced superiority in methanol economy and thermal efficiency relative to the stoichiometric engine. This performance discrepancy can be explained by differences in in-cylinder combustion. The stoichiometric combustion strategy yields high in-cylinder combustion temperature, leading to substantial heat losses via heat transfer and exhaust, which limits the effective power output. In comparison, the lean-burn strategy maintains a lower in-cylinder temperature, which mitigates the heat transfer and exhaust losses [37,38]. Consequently, a higher proportion of combustion heat is converted into effective power output. Furthermore, the lean-burn engine is designed with a higher compression ratio than the stoichiometric engine, which is also a possible reason for its improved fuel economy and thermal efficiency. On the one hand, an increased compression ratio elevates the in-cylinder pressure and temperature at the end of the compression stroke, which facilitates shortening ignition delay and optimizing combustion phasing, further improving power output [39]. On the other hand, higher octane ratings and greater heat of vaporization of methanol make it appropriate for high-compression-ratio engines [40]. Quantitatively, the lean-burn strategy reduces methanol consumption by 6.11% under cold-start conditions and 5.98% under hot-start conditions relative to the stoichiometric strategy, which means that the lean-burn strategy could partially compensate for and even offset the disadvantage of the stoichiometric methanol engine in fuel consumption compared to the diesel engine, further indicating that the lean-burn strategy is a promising technical route for heavy-duty methanol engines to achieve carbon reduction.

Table 1. Fuel consumption of methanol engines.

		Stoichiometric		**Lean-Burn**	
		Cold-Start	**Warm-Start**	**Cold-Start**	**Warm-Start**
CO	mg/(kW·h)	25,169.41	21,672.57	5252.47	4352.25
NMHC	mg/(kW·h)	3354.35	2156.78	3224.41	2721.67
CH_4	mg/(kW·h)	24.15	4.81	0.00	0.00
CO_2	g/(kW·h)	666.03	650.70	654.20	636.00
Fuel consumption	g/(kW·h)	516.55	500.17	485.01	470.24
Thermal efficiency	%	30.70	31.71	32.70	33.73

3.2. Gaseous Pollutants

Figures 2–4 plot the regulated pollutant (including CO, NMHC, and NO_x) emissions from stoichiometric and lean-burn methanol engines under cold-start and hot-start condi-

tions. As seen in Figure 2, compared with the stoichiometric engine, the lean-burn engine exhibits a significantly lower raw and post-catalyst CO emissions under both cold-start and hot-start conditions. This difference can be explained from two perspectives. On the one hand, the lean-burn engine maintains excess O_2 inside the cylinder and operates at a higher compression ratio. The excessive O_2 provides sufficient oxidant to support methanol combustion. A higher compression ratio raises the in-cylinder pressure and temperature at the end of the compression stroke. Both factors facilitate complete methanol combustion and thereby lower raw exhaust CO emissions. On the other hand, the calculated CO conversion efficiency reaches no less than 85% for the stoichiometric engine and 91% for the lean-burn engine. This indicates that the oxidation catalyst of the lean-burn engine achieves higher CO conversion efficiency than the TWC used in the stoichiometric engine. This is because excess O_2 is available as the oxidant for CO oxidation in the OC of the lean-burn engine. By contrast, only limited O_2 and NO_x act as oxidants for CO conversion in the TWC of the stoichiometric engine. Furthermore, the stoichiometric engine produces extremely high raw exhaust CO emissions. To satisfy emission regulations, its TWC must maintain high conversion efficiencies of at least 84% under cold-start conditions and 82% under hot-start conditions, imposing stringent durability demands on the TWC. In comparison, raw exhaust CO emissions from the lean-burn engine are close to the regulated CO emission limit (4000 mg/(kW·h)). So long as the OC achieves CO conversion efficiencies of no less than 24% under cold-start conditions and 9% under hot-start conditions, the CO emissions from the lean-burn engine can comply with regulatory limits. This suggests that the aftertreatment system of the lean-burn methanol engine possesses superior durability for CO emission control.

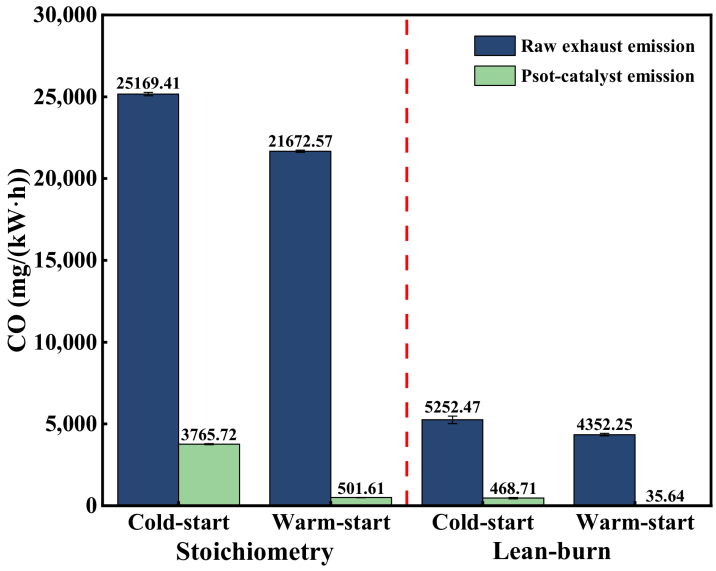


Figure 2. CO emission.

As seen in Figure 3, no significant difference in NMHC emissions is observed between stoichiometric and lean-burn engines under cold-start conditions. This phenomenon is mainly attributed to the fuel-switching strategy commonly adopted by methanol engines. Methanol exhibits a high latent heat of vaporization, which results in poor fuel volatility under cold-start conditions and further inhibits in-cylinder fuel–air mixture formation. Therefore, the methanol engine in this study is initially fueled with gasoline under cold-start conditions and subsequently switched to methanol once the coolant temperature reaches 70 °C. The NMHC emissions generated during the cold-start WHTC are primarily incomplete oxidation products of gasoline. The calculated NMHC conversion efficiency is

no less than 92% for both stoichiometric and lean-burn engines, indicating that TWC and OC achieve equivalent catalytic conversion of NMHC emissions and thus yield similar NMHC emission levels for the two engine modes. However, the lean-burn engine produces higher NMHC emissions than the stoichiometric engine under hot-start conditions. Considering that nearly no fuel switching or air–fuel enrichment occurs under hot-start conditions, the NMHC emission difference between the two engine modes is mainly attributed to discrepancies in methanol combustion behavior. Specifically, the excess O_2 in lean-burn engines produces extensive ultra-lean air–fuel mixtures, causing more NMHC intermediate products to fail to achieve complete oxidation and be directly exhausted. Given the high raw NMHC exhaust emissions, compliance with the regulatory limit of 160 mg/(kW·h) for both engine modes requires excellent catalytic performance of the aftertreatment systems, with a conversion efficiency of no less than 95% under cold-start conditions and 93% under hot-start conditions. These analyses indicate that NMHC emission control poses a severe challenge for methanol engines to satisfy increasingly stringent emission regulations.

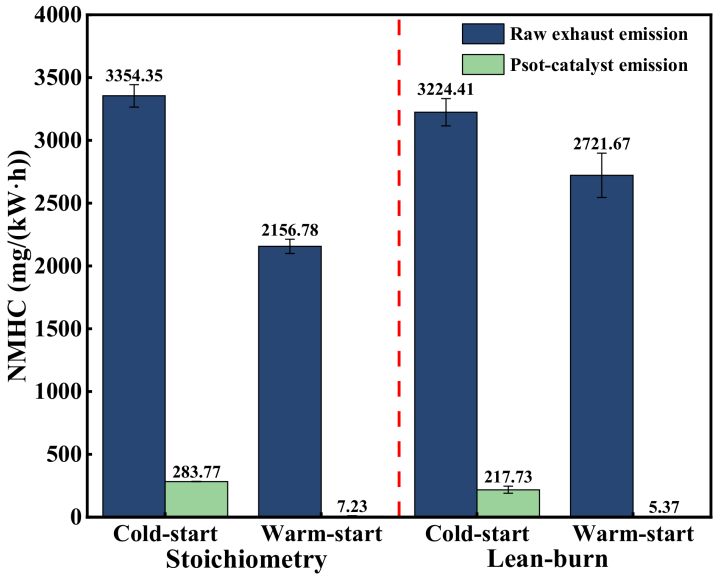


Figure 3. NMHC emission.

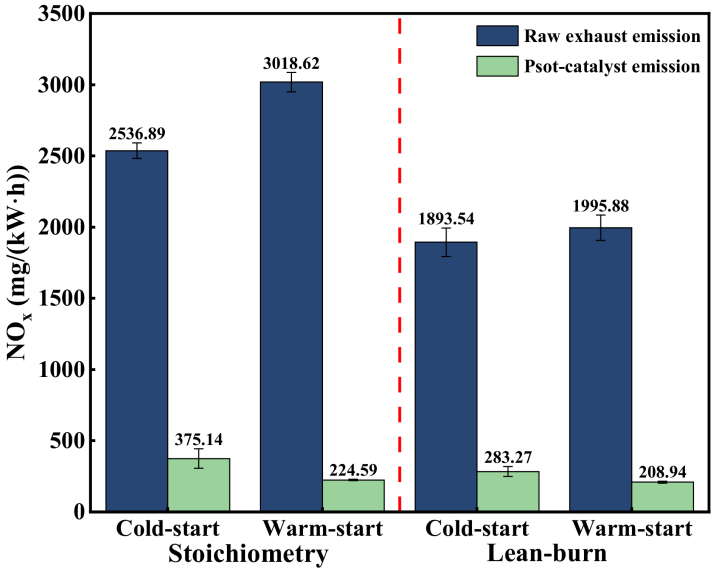


Figure 4. NO_X emission.

As seen in Figure 4, the lean-burn methanol engine exhibits a significant advantage in NO_x emissions compared with the stoichiometric engine. Theoretically, in-cylinder NO_x formation is mainly governed by in-cylinder temperature, O_2 availability, and residence time within the reaction zone [41]. Although the stoichiometric and lean-burn engines are tested over the same driving cycle, the lean-burn engine operates at a higher rated speed than the stoichiometric engine, which leads to shorter residence time of reactants inside the reaction zone for the lean-burn engine and thereby limits NO_x formation. Furthermore, the ultra-lean air–fuel mixture yields lower in-cylinder temperatures in the lean-burn engine, which also suppresses NO_x formation. Although the lean-burn engine provides greater O_2 availability, which facilitates NO_x formation, the shorter residence time in the reaction zone and lower in-cylinder temperature act as the dominant factors inhibiting NO_x formation. Furthermore, although post-catalyst NO_x emissions of both stoichiometric and lean-burn engines can meet the regulatory limit of 460 mg/(kW·h), a notable difference exists in the required catalytic performance between the two engine modes. The lean-burn engine demands a conversion efficiency of no less than 77%, while the stoichiometric engine requires no less than 85%. This indicates that the lean-burn methanol engine imposes less stringent requirements for developing matching aftertreatment systems and exhibits a lower NO_x emission compliance risk relative to the stoichiometric engine.

3.3. Particulate Matter

Figure 5 plots the PM and PN emissions from stoichiometric and lean-burn methanol engines under cold-start and hot-start conditions. As presented above, the lean-burn engine achieves lower PM and PN emissions than the stoichiometric engine. This discrepancy can be explained from two perspectives. On the one hand, the lean-burn strategy improves in-cylinder O_2 availability, which supplies sufficient oxidant for fuel combustion. In addition, the lean-burn engine adopts a higher compression ratio, which increases the in-cylinder pressure and temperature at the end of the compression stroke and facilitates complete fuel combustion. Both factors help reduce raw particulate emissions. On the other hand, an oxidation catalyst is usually arranged upstream of the particulate filter on the lean-burn engine, which can convert NO into NO_2 under lean conditions. The generated NO_2 acts as an oxidant to promote continuous passive regeneration of soot accumulated in the downstream particulate filter [42]. This maintains a stable filtration efficiency and thereby reduces post-catalyst particulate emissions. Furthermore, it is worth noting that the reduction in PM is relatively modest, whereas the PN reduction exceeds one order of magnitude. This reveals that large-sized particulates, which dominate the total particulate mass, account for only a small fraction of all particulates. It is also observed that both stoichiometric and lean-burn methanol engines produce substantially lower PM and PN emissions under hot-start conditions than under cold-start conditions. This can be attributed to the fact that each methanol molecule contains only one methyl group. Compared with other carbon-based fuels, methanol is less likely to form particulate precursors (e.g., carbon–carbon unsaturated bonds and benzene rings) during combustion. Accordingly, particulate emissions are mainly produced during cold-start and warm-up stages when the fuel enrichment strategy is activated. Furthermore, it is noted that the lean-burn methanol engine can meet the PN regulatory limit (6×10^{11}) without aftertreatment systems. In contrast, the stoichiometric engine still risks exceeding this PN limit even when equipped with aftertreatment devices, which further highlights the superiority of lean-burn methanol engines in particulate emissions.

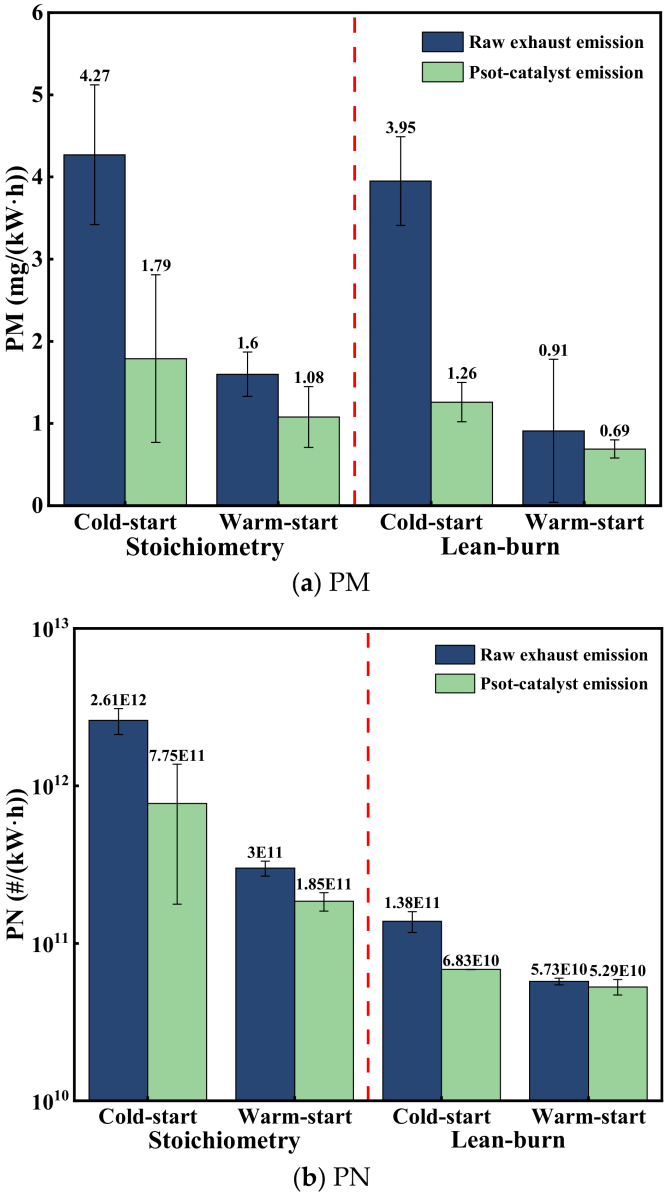
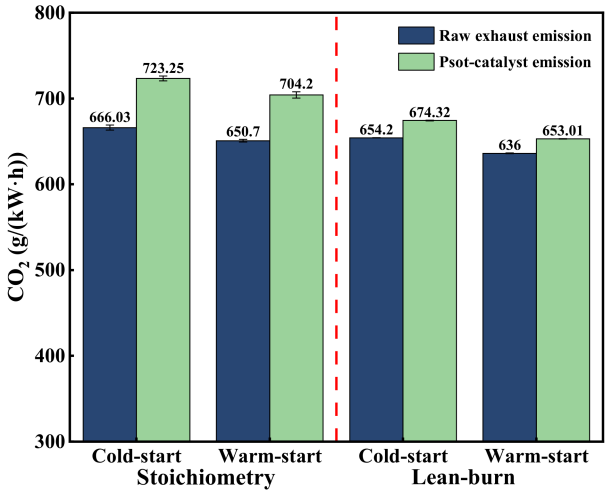


Figure 5. Particulate matter emission. (# denotes particle number).

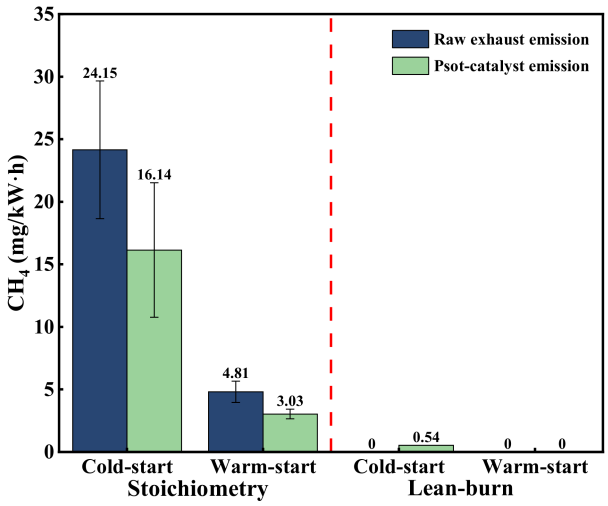
3.4. Greenhouse Gases

Figure 6 plots the greenhouse gas emissions (including CO_2 and CH_4) of stoichiometric and lean-burn methanol engines. As seen in Figure 6a, the lean-burn methanol engine exhibits a slight advantage in raw exhaust CO_2 emissions compared with the stoichiometric engine, with a reduction of 1.78% under cold-start conditions and 2.26% under hot-start conditions. Theoretically, lean-burn engines provide sufficient O_2 for methanol combustion, which is expected to promote greater CO_2 formation. In practice, the ultra-lean air–fuel mixture reduces the in-cylinder temperature, increases the wall quenching distance, and thereby yields substantial incomplete combustion products. On the other hand, the relatively low exhaust temperature of lean-burn engines weakens the secondary oxidation of incomplete combustion products within the aftertreatment system. These two factors jointly result in slightly lower raw exhaust CO_2 emissions from lean-burn engines. Furthermore, it is noted that although post-catalyst CO_2 emissions increase for both engine modes relative to raw exhaust emissions, the CO_2 emission advantage of lean-burn engines is further amplified, reaching 6.77% under cold-start conditions and 7.27% under hot-start conditions. This increase in CO_2 emissions is mainly attributed to elevated fuel

consumption and catalytic reactions within aftertreatment systems. On the one hand, the installation of aftertreatment systems inevitably increases engine backpressure, which raises fuel consumption. On the other hand, aftertreatment systems convert CO, NMHC, and other incomplete combustion products into CO_2. Furthermore, the backpressure increment caused by aftertreatment systems in lean-burn engines is lower than that in stoichiometric engines. This leads to milder fuel consumption deterioration for lean-burn modes and further strengthens their superiority in CO_2 emission performance.



(**a**) CO_2 emission



(**b**) CH_4 emission

Figure 6. Greenhouse gas emissions.

As seen in Figure 6b, the stoichiometric engine produces considerable CH_4 emissions, whereas CH_4 emissions from the lean-burn engine are negligible. For the stoichiometric engine, CH_4, as a key intermediate product of methanol combustion, cannot be fully oxidized due to the limited in-cylinder O_2, thereby generating substantial raw CH_4 emissions. On the other hand, CH_4 features a symmetric tetrahedral structure and high C–H bond energy [43,44], making it difficult to oxidize by NO within the TWC and ultimately resulting in prominent post-catalyst CH_4 emissions. In contrast, for lean-burn engines, sufficient in-cylinder excess O_2 enables CH_4 to be fully oxidized into final products, which directly suppresses raw exhaust CH_4 emissions. Furthermore, although the stoichiometric methanol engine yields far higher CH_4 emissions than the lean-burn engine, its emissions remain well below the regulatory limit of 500 mg/(kW·h). This indicates that methanol engines pose no prominent CH_4 emission compliance risks, especially lean-burn configurations.

Overall, the lean-burn methanol engine exhibits superior total greenhouse gas emission performance compared with the stoichiometric engine.

3.5. Non-Regulated Pollutants

Figure 7 plots the unregulated emissions (including unburned methanol, formaldehyde, and NH_3) of stoichiometric and lean-burn methanol engines under cold-start and hot-start conditions. As seen in Figure 7a,b, the lean-burn engine exhibits substantially higher unburned methanol and formaldehyde emissions under cold-start conditions than the stoichiometric engine, with emission discrepancies of 283% for unburned methanol and 1709% for formaldehyde. This phenomenon is mainly attributed to the difference in raw exhaust emissions between stoichiometric and lean-burn engines. As major intermediate products of methanol combustion, unburned methanol and formaldehyde are primarily generated in low-temperature reaction zones, particularly the quench layer near the cylinder wall. For lean-burn engines, excess air lowers the in-cylinder temperature and enlarges the wall quenching distance. Consequently, more unburned methanol accumulates near the cylinder wall, accompanied by substantial formaldehyde formation. Meanwhile, although lean-burn engines feature higher residual O_2 concentrations, their exhaust temperature is considerably lower than that of stoichiometric engines. This directly inhibits the oxidation of unburned methanol and formaldehyde in aftertreatment systems, resulting in prominent post-catalyst emissions from lean-burn engines. Furthermore, it is noted that unburned methanol and formaldehyde emissions under hot-start conditions are substantially lower than those under cold-start conditions, indicating that these two pollutants are mainly produced during cold-start and warm-up processes. This can be explained by the mandatory fuel enrichment strategy adopted to guarantee stable engine startup during cold-start and warm-up phases. The rich air–fuel mixture inevitably produces abundant unburned methanol and formaldehyde. Meanwhile, the relatively low exhaust temperature during cold-start and warm-up phases prevents aftertreatment systems from achieving efficient pollutant conversion, thereby causing prominent post-catalyst emissions under cold-start conditions.

Both methanol and formaldehyde bring prominent challenges to human health and atmospheric environment. Methanol poses potential health hazards under prolonged inhalation exposure [45] and may cause corrosion of engine metallic components and seals during long-term operation [46]. Formaldehyde is classified as a typical human carcinogen, and long-term inhalation can induce severe irritation and irreversible damage to the human respiratory system [47]. As a highly reactive volatile organic compound in the atmosphere, formaldehyde actively participates in complex photochemical reactions and significantly promotes tropospheric ozone formation, thereby deteriorating urban air quality and exacerbating atmospheric pollution [48]. In this context, the elevated unburned methanol and formaldehyde emission levels of lean-burn methanol engines identified in this study may serve as a critical bottleneck limiting the further popularization and industrial application of such heavy-duty engines. Current mainstream emission standards mainly target conventional regulated pollutants, including NOx, PM, CO, and THC, while unified and explicit regulatory limits for formaldehyde remain absent. Therefore, future revisions of emission standards should fully consider incorporating unburned methanol and formaldehyde into the pollutant regulatory framework. Such standardized emission constraints can effectively drive manufacturers and researchers to mitigate unburned methanol and formaldehyde emissions from lean-burn methanol engines by optimizing in-cylinder combustion parameters, refining fuel injection strategies, and developing high-efficiency, targeted aftertreatment systems for oxygenated pollutant purification. These

improvements will further promote the clean and low-carbon transformation of heavy-duty vehicles and facilitate the sustainable development of road transportation systems.

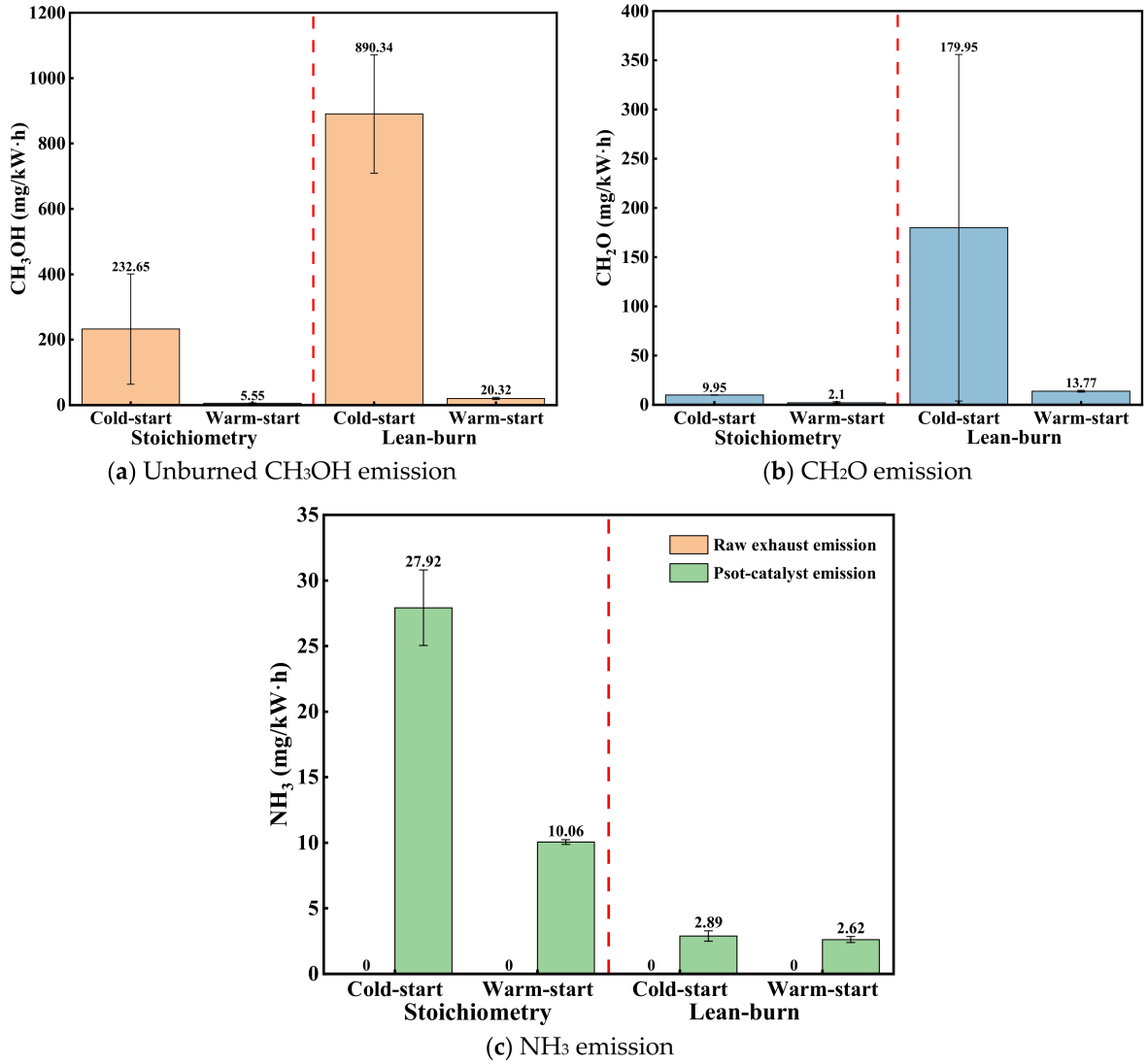


Figure 7. Unregulated emissions.

As seen in Figure 7c, NH_3 only appears in the post-catalyst emissions of both stoichiometric and lean-burn methanol engines, because NH_3 is a typical by-product of the aftertreatment systems for both engine types [49]. For stoichiometric engines equipped with a TWC, NH_3 is produced via side reactions inside the catalyst [50]. Local rich air–fuel zones inevitably form during in-cylinder methanol combustion, generating CO and HC. Within the TWC, CO and HC further react with H_2O to produce H_2 through water–gas shift (WGS) and steam reforming (SR) reactions, respectively [51,52]. The produced H_2 subsequently reacts with exhaust NO to form NH_3 [53]. As illustrated in Figure 7c, the TWC-equipped stoichiometric engine yields higher NH_3 emissions under cold-start conditions than under hot-start conditions. This is because low catalyst temperatures improve the selectivity of NO conversion toward NH_3 formation. As the catalyst temperature rises, the formed NH_3 tends to decompose at elevated temperatures. For lean-burn engines equipped with SCR systems, urea solution serves as the reductant for NO_x abatement. However, excessive urea injection and SCR catalyst aging may cause incomplete NH_3 consumption, allowing unreacted NH_3 to be directly exhausted. Compared with stoichiometric engines, lean-burn engines produce significantly lower NH_3 emissions, with negligible differences between

cold-start and hot-start operating conditions, which demonstrates the superior NH_3 emission performance of lean-burn configurations. Furthermore, this advantage can be further enhanced by improving the accuracy of the urea injection strategy.

3.6. Limitations and Outlook

This study aims to compare the performance of stoichiometric and lean-burn methanol engines. Ideally, well-controlled single-variable experiments require all hardware parameters to remain consistent, with only the combustion strategy modified. However, the two test engines employed in this work differ in compression ratio, aftertreatment configuration, and rated speed, which constitutes an important limitation of the present study. The observed differences in performance and emissions cannot be attributed solely to the combustion strategy, since mismatched hardware parameters may introduce coupled confounding effects. Nevertheless, it should be emphasized that the two engines represent two complete, commercially viable technical routes developed for stoichiometric and lean-burn methanol powertrains, respectively. The matching of compression ratio, rated speed, and aftertreatment scheme represents the optimal design tailored to each combustion mode. Accordingly, the comparison conducted in this work reflects the overall performance disparity between two integrated engineering solutions, rather than an isolated comparison of combustion modes under identical engine hardware conditions. Future research will seek to isolate the influence of combustion strategy by performing tests on a single engine platform with adjustable hardware parameters. This will enable the quantitative decoupling of the effects originating from compression ratio, aftertreatment configuration, and engine speed, and will further deepen the understanding of combustion and emission characteristics of methanol engines.

4. Conclusions

To explore combustion technical routes conducive to carbon reduction and emission control for heavy-duty methanol vehicles, this study selected two China VI-compliant heavy-duty methanol engines adopting stoichiometric combustion and lean-burn strategies as research objects and measured their fuel consumption and exhaust emissions (including regulated pollutants, particulate matter, greenhouse gases and unregulated pollutants) under cold-start and hot-start WHTCs. Subsequently, a comparative analysis of fuel consumption, raw exhaust emissions and aftertreatment catalytic performance was carried out between stoichiometric and lean-burn strategies. The main conclusions are drawn as follows:

(1) The lean-burn strategy reduces methanol consumption by approximately 6% compared with the stoichiometric strategy.

(2) In terms of CO and NO_x emissions, both stoichiometric and lean-burn methanol engines achieve good compliance with emission standards. The lean-burn strategy further markedly cuts raw exhaust emissions and lowers the conversion requirements of aftertreatment systems. For NMHC emissions, emission compliance under cold-start conditions remains the primary challenge, demanding a conversion efficiency of no less than 95%. Although the lean-burn strategy raises raw exhaust NMHC emissions under hot-start conditions, post-catalyst emissions carry no risk of exceeding the regulatory limit.

(3) For particulate emissions, the lean-burn strategy substantially reduces both PM and PN emissions and can meet regulatory limits without aftertreatment systems. In contrast, the stoichiometric engine equipped with aftertreatment devices still risks exceeding the PN regulatory limit under cold-start conditions.

(4) Regarding greenhouse gas emissions, both stoichiometric and lean-burn methanol engines exhibit satisfactory CH_4 emission compliance with standards, and the lean-burn strategy further lowers CO_2 and CH_4 emissions.

(5) In terms of unregulated pollutant emissions, the lean-burn strategy markedly increases emissions of unburned methanol and formaldehyde, particularly under cold-start conditions, yet reduces NH_3 emissions.

Author Contributions: L.S.: Conceptualization, investigation, writing—original draft preparation; C.W.: writing—review and editing, methodology, supervision; J.K.: Resources, project administration; L.L.: Investigation; X.X.: Investigation; D.W.: Investigation; B.L.: Resource; X.W.: Funding, methodology. All authors have read and agreed to the published version of the manuscript.

Funding: This research was funded by National Natural Science Foundation of China (Grant No. 52272342).

Institutional Review Board Statement: Not applicable.

Informed Consent Statement: Not applicable.

Data Availability Statement: The original contributions presented in this study are included in the article. Further inquiries can be directed to the corresponding author.

Conflicts of Interest: Authors Laihua Shi and Xiaoliu Xu were employed by China Merchants Testing Vehicle Technology (Hefei) Co., Ltd., Authors Jianjian Kang, Lan Li, Di Wu and Bing Liu were employed by China Merchants Testing Vehicle Technology Research Institute Co., Ltd. All authors declare that the research was conducted in the absence of any commercial or financial relationships that could be construed as a potential conflict of interest.

Nomenclature

$\Lambda\lambda$	Excess Air Ratio
EF	Emission Factor
$\dot{m}$	Mass Flow Rate
W	Accumulated Work
C	Concentration
M	Molar Mass
q_e	Volume Flow Rate
f	Frequency
$BSFC$	Brake Specific Fuel Consumption
η	Thermal Efficiency
H	Calorific Value
Acronyms	
M	Methanol
NEDC	New European Driving Cycle
WHTC	World Harmonized Transient Cycle
DISI	Direct Injection Spark Ignition
TWC	Three-Way Catalyst
SCR	Selective Catalytic Reduction
OC	Oxidation Catalyst
ASC	Ammonia Slip Catalyst
PM	Particulate Matter
PN	Particulate Number
NMHC	Non-Methane Hydrocarbon
WGS	Water–Gas Shift
SR	Stream Reforming
Subscript	
i	Gaseous Pollutant

References

1. Wang, X.; Dai, M.; Wang, W.; Gao, Y.; Qi, T.; Dong, X.; Ren, P.; Ding, N. Greenhouse gas emissions and peak trend of commercial vehicles in China. *J. Environ. Manag.* **2023**, *331*, 117262. [CrossRef] [PubMed]
2. Institute for Carbon Neutrality, Tsinghua University. *Carbon Neutrality Report*; Institute for Carbon Neutrality, Tsinghua University: Beijing, China, 2024.
3. Wei, Y.; Zhu, Z.; Liu, S.; Liu, H.; Shi, Z.; Zeng, Z. Investigation on injection strategy affecting the mixture formation and combustion of a heavy-duty spark-ignition methanol engine. *Fuel* **2023**, *334*, 126680. [CrossRef]
4. Zhen, X.; Wang, Y. An overview of methanol as an internal combustion engine fuel. *Renew. Sustain. Energy Rev.* **2015**, *52*, 477–493. [CrossRef]
5. Li, C.; Hao, Q.; Wang, H.; Hu, Y.-J.; Xu, G.; Qin, Q.; Wang, X.; Negnevitsky, M. Assessing green methanol vehicles' deployment with life cycle assessment-system dynamics model. *Appl. Energy* **2024**, *363*, 123055. [CrossRef]
6. Tian, Z.; Wang, Y.; Zhen, X.; Liu, Z. The effect of methanol production and application in internal combustion engines on emissions in the context of carbon neutrality: A review. *Fuel* **2022**, *320*, 123902. [CrossRef]
7. Verhelst, S.; Turner, J.W.; Sileghem, L.; Vancoillie, J. Methanol as a fuel for internal combustion engines. *Prog. Energy Combust. Sci.* **2019**, *70*, 43–88. [CrossRef]
8. Dhaliwal, B.; Yi, N.; Checkel, D. *Emissions Effects of Alternative Fuels in Light-Duty and Heavy-Duty Vehicles*; SAE Technical Paper 2000-01-0692; SAE International: Warrendale, PA, USA, 2000.
9. Nuthan Prasad, B.S.; Pandey, J.K.; Kumar, G. Effect of hydrogen enrichment on performance, combustion, and emission of a methanol fueled SI engine. *Int. J. Hydrogen Energy* **2021**, *46*, 25294–25307. [CrossRef]
10. Wei, H.; Zhang, Z.; Zhang, X.; Dong, F.; Yuan, W.; Chen, H. Overview for methanol and formaldehyde unregulated emissions of methanol fueled engines. *J. Energy Inst.* **2025**, *120*, 102089. [CrossRef]
11. Luo, L.; Wang, H.; Li, C.; Hu, Y. Life cycle assessment of methanol vehicles from energy, environmental and economic perspectives. *Energy Rep.* **2022**, *8*, 5487–5500. [CrossRef]
12. Zhu, Z.; Mu, Z.; Wei, Y.; Du, R.; Liu, S. Experimental evaluation of performance of heavy-duty SI pure methanol engine with EGR. *Fuel* **2022**, *325*, 124948. [CrossRef]
13. Yu, W.; Hou, P.; Chen, J.; Ge, Z.; Wang, X.; Ge, Y. Evaluation of pollutant and greenhouse gas emission reduction effect of vehicles burning neat methanol. *Energy* **2026**, *349*, 140629. [CrossRef]
14. Machiele, P.A. *Summary of the Fire Safety Impacts of Methanol as a Transportation Fuel*; SAE Technical Paper 1990-90-1113; SAE International: Warrendale, PA, USA, 1990.
15. Wei, Y.J.; Liu, S.H.; Li, H.S.; Yang, R.; Liu, J.; Wang, Y. Effects of Methanol/Gasoline Blends on a Spark Ignition Engine Performance and Emissions. *Energy Fuels* **2008**, *22*, 1254–1259. [CrossRef]
16. Zhao, H.; Ge, Y.; Hao, C.; Han, X.; Fu, M.; Yu, L.; Shah, A.N. Carbonyl compound emissions from passenger cars fueled with methanol/gasoline blends. *Sci. Total Environ.* **2010**, *408*, 3607–3613. [CrossRef] [PubMed]
17. Zhao, H.; Ge, Y.; Tan, J.; Yin, H.; Guo, J.; Zhao, W.; Dai, P. Effects of different mixing ratios on emissions from passenger cars fueled with methanol/gasoline blends. *J. Environ. Sci.* **2011**, *23*, 1831–1838. [CrossRef] [PubMed]
18. Yao, D.; Ling, X.; Wu, F. Experimental Investigation on the Emissions of a Port Fuel Injection Spark Ignition Engine Fueled with Methanol–Gasoline Blends. *Energy Fuels* **2016**, *30*, 7428–7434. [CrossRef]
19. Wang, X.; Ge, Y.; Liu, L.; Peng, Z.; Hao, L.; Yin, H.; Ding, Y.; Wang, J. Evaluation on toxic reduction and fuel economy of a gasoline direct injection- (GDI-) powered passenger car fueled with methanol–gasoline blends with various substitution ratios. *Appl. Energy* **2015**, *157*, 134–143. [CrossRef]
20. Wang, X.; Ge, Y.; Liu, L.; Gong, H. *Regulated, Carbonyl Emissions and Particulate Matter from a Dual-Fuel Passenger Car Burning Neat Methanol and Gasoline*; SAE Technical Paper 2015-01-1082; SAE International: Warrendale, PA, USA, 2015.
21. Su, S.; Ge, Y.; Wang, X.; Zhang, M.; Hao, L.; Tan, J.; Shi, F.; Guo, D.; Yang, Z. Evaluating the In-Service Emissions of High-Mileage Dedicated Methanol-Fueled Passenger Cars: Regulated and Unregulated Emissions. *Energies* **2020**, *13*, 2680. [CrossRef]
22. Guo, J.; Ge, Y.; Hao, L.; Tan, J.; Li, J.; Feng, X. On-road measurement of regulated pollutants from diesel and CNG buses with urea selective catalytic reduction systems. *Atmos. Environ.* **2014**, *99*, 1–9. [CrossRef]
23. Rosero, F.; Fonseca, N.; López, J.-M.; Casanova, J. Effects of passenger load, road grade, and congestion level on real-world fuel consumption and emissions from compressed natural gas and diesel urban buses. *Appl. Energy* **2021**, *282*, 116195. [CrossRef]
24. Duan, X.; Feng, L.; Liu, H.; Jiang, P.; Chen, C.; Sun, Z. Experimental investigation on exhaust emissions of a heavy-duty vehicle powered by a methanol-fuelled spark ignition engine under World Harmonized Transient Cycle and actual on-road driving conditions. *Energy* **2023**, *282*, 128869. [CrossRef]
25. Feng, L.; Chu, X.; He, J.; Duan, X.; Sun, Z. The performance and emissions behaviors of methanol heavy-duty vehicle under cold start and hot start of the WHTC standard condition. *Energy* **2024**, *309*, 133169. [CrossRef]
26. Liu, J.; Dumitrescu, C.E. Combustion partitioning inside a natural gas spark ignition engine with a bowl-in-piston geometry. *Energy Convers. Manag.* **2019**, *183*, 73–83. [CrossRef]

27. Duan, Q.; Li, T.; Liu, D.; Yin, X.; Zeng, K.; Wang, L. Improving the lean burn performance of a high compression ratio methanol engine by multiple-injection. *Appl. Therm. Eng.* **2024**, *236*, 121481. [CrossRef]
28. Zhang, M.; Cao, J. Effects of Lean Burn on Combustion and Emissions of a DISI Engine Fueled with Methanol–Gasoline Blends. *Energies* **2024**, *17*, 4023. [CrossRef]
29. Gong, C.; Li, Z.; Chen, Y.; Liu, J.; Liu, F.; Han, Y. Influence of ignition timing on combustion and emissions of a spark-ignition methanol engine with added hydrogen under lean-burn conditions. *Fuel* **2019**, *235*, 227–238. [CrossRef]
30. Badawy, T.; Panithasan, M.S.; Turner, J.W.G.; Kim, J.; Han, D.; Lee, J.; AlRamadan, A.S.; Chang, J. Performance and emissions evaluation of a multi-cylinder research engine fueled with ethanol, methanol, gasoline Euro-6, E85, and iso-stoichiometric ternary GEM mixtures operated at lean conditions. *Fuel* **2024**, *363*, 130962. [CrossRef]
31. Gong, C.; Li, Z.; Yi, L.; Liu, F. Comparative study on combustion and emissions between methanol port-injection engine and methanol direct-injection engine with H2-enriched port-injection under lean-burn conditions. *Energy Convers. Manag.* **2019**, *200*, 112096. [CrossRef]
32. Ning, L.; Duan, Q.; Liu, B.; Zeng, K. Experimental assessment of lean-burn characteristics for a modified diesel engine operated in methanol direct injection spark ignition (DISI) mode at full throttle condition. *Fuel* **2020**, *279*, 118455. [CrossRef]
33. Wu, B.; Wang, L.; Shen, X.; Yan, R.; Dong, P. Comparison of lean burn characteristics of an SI engine fueled with methanol and gasoline under idle condition. *Appl. Therm. Eng.* **2016**, *95*, 264–270. [CrossRef]
34. Gong, C.; Li, D.; Liu, J.; Liu, F. Computational study of excess air ratio impacts on performances of a spark-ignition H2/methanol dual-injection engine. *Energy* **2024**, *289*, 130059. [CrossRef]
35. Gong, C.; Zhang, Z.; Sun, J.; Liu, F. Optimization on timings of injection and spark of a high compression-ratio stratified-charge methanol engine under ultra-lean burn. *Fuel* **2021**, *285*, 119227. [CrossRef]
36. Gong, C.; Peng, L.; Chen, Y.; Liu, J.; Liu, F.; Han, Y. Computational study of intake temperature effects on mixture formation, combustion and unregulated emissions of a DISI methanol engine during cold start. *Fuel* **2018**, *234*, 1269–1277. [CrossRef]
37. Hong, B.; Lius, A.; Mahendar, S.K.; Mihaescu, M.; Cronhjort, A. Energy and exergy characteristics of an ethanol-fueled heavy-duty SI engine at high-load operation using lean-burn combustion. *Appl. Therm. Eng.* **2023**, *224*, 120063. [CrossRef]
38. Kim, K.Y.; Lee, S.; Lee, S.H.; Kim, S.J.; Min, K.D.; Lee, J.W. Effects of Various Bore–Stroke Ratios on Hydrogen Direct Injection Spark Ignition Engines with Variable Valve Timing Under Low-Load Conditions. *Int. J. Automot. Technol.* **2025**, *26*, 35–45. [CrossRef]
39. Gong, C.; Liu, F.; Sun, J.; Wang, K. Effect of compression ratio on performance and emissions of a stratified-charge DISI (direct injection spark ignition) methanol engine. *Energy* **2016**, *96*, 166–175. [CrossRef]
40. Arapatsakos, C.I.; Karkanis, A.N.; Sparis, P.D. *Behavior of a Small Four-Stroke Engine Using as Fuel Methanol-Gasoline Mixtures*; SAE Technical Paper 2003-32-0024; SAE International: Warrendale, PA, USA, 2003.
41. Scappin, F.; Stefansson, S.H.; Haglind, F.; Andreasen, A.; Larsen, U. Validation of a zero-dimensional model for prediction of NOx and engine performance for electronically controlled marine two-stroke diesel engines. *Appl. Therm. Eng.* **2012**, *37*, 344–352. [CrossRef]
42. Chen, C.; Yao, A.; Yao, C.; Qu, G. Experimental study of the active and passive regeneration procedures of a diesel particulate filter in a diesel methanol dual fuel engine. *Fuel* **2020**, *264*, 116801. [CrossRef]
43. Kang, S.B.; Nam, S.B.; Cho, B.K.; Nam, I.-S.; Kim, C.H.; Oh, S.H. Effect of speciated HCs on the performance of modern commercial TWCs. *Catal. Today* **2014**, *231*, 3–14. [CrossRef]
44. Wang, X.; Wang, C.; Li, R.; Ge, Y.; Hao, L.; Tan, J. Tracing the regulated emissions of field-aged gasoline/natural gas bi-fuel taxis from new to 160,000 km: Deterioration and environmental implications. *Fuel* **2024**, *362*, 130863. [CrossRef]
45. Mojica, C.V.; Pasol, E.A.; Dizon, M.L.; Kiat, W.A., Jr.; Lim, T.R.; Dominguez, J.C.; Valencia, V.V.; Tuaño, B.J.P. Chronic methanol toxicity through topical and inhalational routes presenting as vision loss and restricted diffusion of the optic nerves on MRI: A case report and literature review. *Eneurologicalsci* **2020**, *20*, 100258. [CrossRef] [PubMed]
46. Geng, Z.; Li, J.; Deng, Y.; Li, W.; Ampah, J.D.; Xu, T.; Jin, C.; Liu, H. Effects of methanol fuel and its combustion products on the corrosion performance of engine aluminum alloy materials. *Fuel* **2026**, *427*, 139907. [CrossRef]
47. Khoshakhlagh, A.H.; Mohammadzadeh, M.; Manafi, S.S.; Yousefian, F.; Gruszecka-Kosowska, A. Inhalational exposure to formaldehyde, carcinogenic, and non-carcinogenic risk assessment: A systematic review. *Environ. Pollut.* **2023**, *331*, 121854. [CrossRef] [PubMed]
48. Olaguer, E.P.; Hu, Y.; Kilmer, S.; Adelman, Z.E.; Vasilakos, P.; Odman, M.T.; Vaerten, M.; McDonald, T.; Gregory, D.; Lomerson, B.; et al. Is There a Formaldehyde Deficit in Emissions Inventories for Southeast Michigan? *Atmosphere* **2023**, *14*, 461. [CrossRef]
49. Ge, Z.; Wang, C.; Ji, Z.; Wang, Y.; Yang, L.; Huang, Y.; Lyu, L. Research on real-road NH_3 emissions of China-6 heavy-duty natural gas and diesel vehicles. *J. Hazard. Mater.* **2025**, *489*, 137583. [CrossRef] [PubMed]
50. Li, R.; Wang, C.; Wang, X.; Luo, J.; Yin, D.; Wen, M.; Hao, L.; Tan, J.; Ge, Y. On-road measurement of post-catalyst ammonia emissions from gasoline and hybrid vehicles using quantum cascade laser detector. *Environ. Pollut.* **2025**, *364*, 125319. [CrossRef] [PubMed]

51. González-Velasco, J.R.; Botas, J.A.; González-Marcos, J.A.; Gutiérrez-Ortiz, M.A. Influence of water and hydrocarbon processed in feedstream on the three-way behaviour of platinumalumina catalysts. *Appl. Catal. B Environ.* **1997**, *12*, 61–79. [CrossRef]
52. Qian, Y.; Wei, X.; Sun, Y.; Tang, F.; Meng, S.; Qiu, L.; Wang, T.; Ye, B.; Pan, T.; Zhang, Y. Investigation of the formation characteristics of N_2O and NH_3 for stoichiometric natural gas engines with Pd-only catalyst. *Fuel* **2022**, *329*, 125223. [CrossRef]
53. Wang, C.; Wang, X.; Tan, J.; Dong, C.; Hou, L.; Feng, J.; Ge, Y. Investigation of Engine Exhaust Conversion and N_2O/NH_3 Generation on Pd-Based Catalyst. *Atmosphere* **2025**, *16*, 1038. [CrossRef]

Disclaimer/Publisher's Note: The statements, opinions and data contained in all publications are solely those of the individual author(s) and contributor(s) and not of MDPI and/or the editor(s). MDPI and/or the editor(s) disclaim responsibility for any injury to people or property resulting from any ideas, methods, instructions or products referred to in the content.